Astron. Astrophys. 334, 482–488 (1998)

ASTRONOMY AND ASTROPHYSICS

Mid-infrared spectroscopy of obscured IRAS galaxies⋆

Hideaki Mouri[1], **Yoshiaki Taniguchi**[2], **Yasunori Sato**[3,4], **and Kimiaki Kawara**[5]

[1] Meteorological Research Institute, 1-1 Nagamine, Tsukuba 305, Japan
[2] Astronomical Institute, Tohoku University, Aoba, Sendai 980-77, Japan
[3] ISO Science Operations Centre, Astrophysics Division of European Space Agency, E-28080 Madrid, Spain
[4] Institute of Space and Astronautical Science, 3-1-1 Yoshinodai, Sagamihara, Kanagawa 220, Japan
[5] Institute of Astronomy, University of Tokyo, Mitaka, Tokyo 181, Japan

Received 6 January 1998 / Accepted 24 February 1998

Abstract. Spectra from 6 to 12 μm are presented for the infrared galaxies NGC 1266, Arp 148, and IRAS 1713+53. Though they are not markedly luminous ($\leq 10^{12}L_{\odot}$), their IRAS colors are close to the colors of ultraluminous infrared galaxies, and thus indicative of heavy obscuration. The 6–12 μm spectra are dominated by emission features of polycyclic aromatic hydrocarbon molecules at 6.2, 7.7, and 8.6 μm. This demonstrates the existence of dust-enshrouded starbursts in those galaxies.

Key words: galaxies: ISM – galaxies: starburst – infrared: galaxies – infrared: ISM: lines and bands

1. Introduction

The Infrared Astronomical Satellite (IRAS) discovered many luminous galaxies radiating the bulk of their energy in the infrared (IR). The IRAS colors of these IR galaxies are often close to blackbody spectra, indicating that the energy sources, i.e., OB stars or active galactic nuclei (AGNs), are highly obscured and their radiation is converted into thermal dust emission (Baan 1989; Condon et al. 1991; Helou et al. 1991; Majewski et al. 1993). A well-studied example is a class of ultraluminous IR galaxies ($L_{\rm IR} = L_{8-1000\mu{\rm m}} > 10^{12}L_{\odot}$, Sanders & Mirabel 1996 and references therein). However, little attention has been paid to the less-luminous obscured galaxies. Their energy sources are still uncertain. We observe emission features at 6.2, 7.7, and 8.6 μm in such objects (NGC 1266, Arp 148, and IRAS 1713+53), in order to explore the contribution of OB stars to the IR luminosities, by using the Infrared Space Observatory (ISO, Kessler et al. 1996).

The emission features at 3.28, 3.4, 6.2, 7.7, 8.6, and 11.3 μm are due to transient heating of polycyclic aromatic hydrocarbon molecules (PAHs) by UV photons from OB stars (Puget & Léger 1989). The intensity ratio of the 3.28 μm feature to the IR continuum is constant among starburst galaxies (Mouri et al. 1990; Dennefeld & Désert 1990). This implies that the fluxes of PAH features are proportional to the total stellar output before it is absorbed by dust grains. On the other hand, the features are absent in AGNs, where PAHs are destroyed by X-rays (Désert & Dennefeld 1988). Hence PAH features are useful in evaluating the contribution of OB stars to the IR luminosities. In particular, PAH features at 6.2, 7.7, and 8.6 μm are insensitive to the extinction, and hence suited to probing sources buried in dust. For instance, extinction at 6.2 μm (0.022 $A_{\rm V}$, Mathis 1990) is as small as that in the hard X-ray range (0.01 $A_{\rm V}$, Rieke 1988). The ISO has provided us with an opportunity to study the PAH features at 6.2, 7.7, and 8.6 μm, which are not accessible from the ground.

The plan of our paper is as follows. The selection of the program galaxies are described in Sect. 2. The observation and the data reduction are described in Sect. 3. The results are presented in Sect. 4, and compared with the data of the archetypical starburst system M 82 in Sect. 5. Finally, a brief summary is given in Sect. 6.

2. Sample selection

The program galaxies are selected from the IRAS Bright Galaxy Survey (BGS), which covers 83 % of the sky and contains all the 601 sources brighter than 5.24 Jy at 60 μm (Soifer et al. 1989; Sanders et al. 1995). The selection is based on the spectral curvature at 60 μm (C_{60}, Condon et al. 1991) and the ratio of the monochromatic flux at 12 μm to the far-IR flux between 40 and 120 μm ($12/FIR$, Helou et al. 1991):

$$C_{60} = \frac{\log(f_{60}/f_{100})}{\log(100/60)} - \frac{\log(f_{25}/f_{60})}{\log(60/25)}\,, \qquad (1)$$

and

$$\frac{12}{FIR} = \frac{F_{12}}{F_{\rm FIR}} = \frac{2.5\times10^{-13}f_{12}}{3.25\times10^{-14}f_{60}+1.26\times10^{-14}f_{100}}\,, \qquad (2)$$

where f_{λ} is the flux density at λ μm in janskys measured by IRAS.

Send offprint requests to: H. Mouri, (hmouri@mri-jma.go.jp)

⋆ Based on observations with the Infrared Space Observatory, an ESA project with instruments funded by ESA Member States (especially the PI countries: France, Germany, the Netherlands, and the United Kingdom) with the participation of ISAS and NASA.

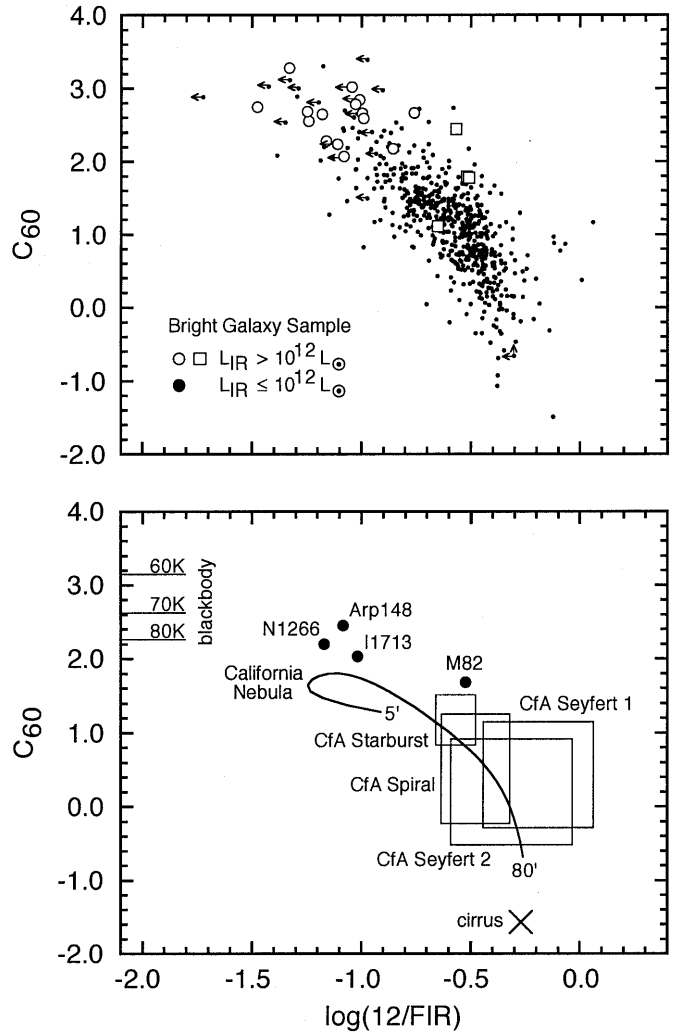

Fig. 1. Diagrams of C_{60} versus $12/FIR$. The upper panel is for BGS galaxies. Open squares are objects with $L_{\rm IR} > 10^{12}\,L_\odot$ and $f_{25}/f_{60} > 0.2$. Open circles are objects with $L_{\rm IR} > 10^{12} L_\odot$ and $f_{25}/f_{60} \le 0.2$. Filled circles are objects with $L_{\rm IR} \le 10^{12} L_\odot$. The lower panel shows the 1σ dispersion boxes of CfA Seyferts, starbursts, and normal spirals. A cross represents the cirrus spectrum of our Galaxy. A solid curve represents the local spectra of the California Nebula. We also indicate the C_{60} values of blackbody with color temperatures of 60–80 K. Their $12/FIR$ values are too small to be shown in the diagram.

Fig. 1 is a set of the diagrams of C_{60} versus $12/FIR$. The upper panel shows BGS galaxies with $L_{\rm IR} > 10^{12} L_\odot$ (open symbols) and those with $L_{\rm IR} \le 10^{12} L_\odot$ (filled symbols)[1]. Here we have distinguished 15 cool ultraluminous galaxies with $f_{25}/f_{60} \le 0.2$ (circles) from 4 warm ultraluminous galaxies with $f_{25}/f_{60} > 0.2$ (squares), after Sanders et al. (1988). The lower panel shows the 1σ dispersion boxes of Seyferts (Huchra & Burg 1992; Osterbrock & Martel 1993), starbursts (Balzano 1983), and normal spirals from type S0/a to Sm in the CfA catalog (Huchra et al. 1983; Thuan & Sauvage 1992). This panel also shows the cirrus spectrum of our Galaxy (cross, Boulanger & Pérault 1988), and the local spectra of the California Nebula, a reflection nebula around an O7.5 star, at distances to the central star going from 5′ to 80′ (solid curve, Boulanger et al. 1988).

When the IR optical depth is low, IRAS colors are determined by the strength of the radiation (Boulanger et al. 1988). The 12 and 25 μm emissions arise from "small grains" (PAHs and/or other giant molecules), which are transiently heated by single UV photons. On the other hand, the 60 and 100 μm emissions arise from "large grains", which are in thermal equilibrium with the ambient radiation. If the strength of the radiation is increased, large grains become warmer, so that the emission peak is shifted to shorter wavelengths. In addition, the destruction of the smallest grains reduces the emission at 12 μm. Consequently, C_{60} is increased while $12/FIR$ is decreased, as shown by the spectra of the cirrus and the California Nebula. If the radiation strength is increased still more, large grains become to radiate at 12 and 25 μm. This explains the turnover of the locus of the California Nebula at the upper-left corner.

Most of BGS galaxies in Fig. 1 constitute a sequence that follows the colors of the California Nebula. The IR optical depth is low in those galaxies. Scatter of the galaxies is due to the changes in the content of small grains (Helou et al. 1991) and to the additional emission from hot dust particles in the vicinity of ionizing stars (Mouri et al. 1997) or AGNs.

When the IR optical depth is high, the emission is absorbed and reradiated at longer wavelengths. Few clues are left as to the nature of the original energy sources. The IRAS color approaches to a blackbody color, i.e., high C_{60} and low $12/FIR$. This is the situation of cool ultraluminous IR galaxies (Baan 1989; Condon et al. 1991; Helou et al. 1991; Majewski et al. 1993). Most of them (12 objects) exhibit $C_{60} > 2.00$ and $\log(12/FIR) \le -1.00$. These values are far from the values observed in CfA galaxies, and are not found in the spectra of the California Nebula. Fig. 1a contains 28 less-luminous sources with $C_{60} > 2.00$ and $\log(12/FIR) \le -1.00$ (Appendix). From these objects, we have selected our program galaxies, NGC 1266, Arp 148, and IRAS 1713+53, taking account of the observational feasibility.

3. Observation and data reduction

The observations were carried out with the spectrometer ISOPHOT-SL on board the ISO (Lemke et al. 1996). This instrument is non-scanning, has a linear array of 64-element Si:Ga detectors, and covers wavelengths from 5.8 to 11.6 μm. The resolution is $\lambda/\delta\lambda \sim 95$. The field of view is $24'' \times 24''$.

NGC 1266, Arp 148, and IRAS 1713+53 were observed, respectively, during the revolutions 283 (26 August 1996), 169 (4 May 1996), and 277 (20 August 1996). The beam was placed on the optical nucleus in each case. Triangular chopping was

[1] The IR flux is defined as $F_{\rm IR} = 1.8 \times 10^{-14}(13.48 f_{12} + 5.16 f_{25} + 2.58 f_{60} + f_{100})$ W m^{-2} (Sanders & Mirabel 1996). The galaxy distances are computed from the redshifts, with the Hubble constant of 75 km s^{-1} Mpc^{-1} and the deceleration parameter of 0.5, after correcting for the solar motion of 300 km s^{-1} with respect to the centroid of the Local Group. The redshifts are from Soifer et al. (1989) or Sanders et al. (1995). For some nearby galaxies, we instead use the distances listed in their tables.

made with throws of 75″–105″. The throws and directions of the chopping were determined so as to avoid the galaxies themselves and the nearby stars. The on-source integration times were, respectively, 1024, 2048, and 1024 sec.

The data were reduced with the software package ISOPHOT Interactive Analysis, V6.4[2], starting from Edited Raw Data, which had been generated by the pipeline Off-Line Processing V5.0 (Lemke et al. 1996 and the references therein). We applied a linearity correction for the detector pixels, subtracted the dark current, removed cosmic-ray glitches at the 2σ level of the signal fluctuation, corrected for the detector drifts with a stability recognition algorithm, and subtracted the sky background. The flux calibration was made on the basis of the default spectral response function in the package. The uncertainties associated with the calibration are about 30 % at the present stage (Klaas et al. 1997).

4. Results

Fig. 2 illustrates our observational results. The spectrum of NGC 1266 is very noisy, but PAH features at 6.2 and 7.7 μm are surely present. The spectra of Arp 148 and IRAS 1713+53 are of satisfactory quality. The features at 6.2, 7.7, and 8.6 μm are clearly seen in both the galaxies. The tail of the 11.3 μm feature is also discernable in Arp 148. There is an underlying plateau-like continuum between 6 and 9 μm, which could arise from certain small grains (Cohen et al. 1986; Bregman et al. 1989). The continuum emission is very weak between the 8.6 and 11.3 μm features. This could be partly due to the silicate absorption at 9.7 μm.

The spectra are decomposed by fitting the emission features with Gaussians and the continuum with a third-order polynomial (Boulanger et al. 1996), on the basis of the Levenberg-Marquardt algorithm (Press et al. 1992). The decomposition of the spectrum of Arp 148 is restricted to the wavelengths shorter than 10.81 μm, in order to avoid the effect of the 11.3 μm feature. The results are shown in Fig. 3 and Table 1. Relative intensities of the features are consistent with those observed in Galactic objects (Cohen et al. 1986). Since, however, we have assigned somewhat arbitrary shapes to the features and continuum, the formal errors given in Table 1 might underestimate the true uncertainties on the feature fluxes. Hereafter, we focus on the 6.2 μm feature, which seems to have been separated from the continuum better than the other features (Fig. 3).

5. Discussion

The presence of prominent PAH features implies the substantial contribution of OB stars to the IR luminosities of our program galaxies. Here the flux of the 6.2 μm feature ($F_{6.2}$) is compared with the IR flux from 8 to 1000 μm ($F_{\rm IR}$) and the Brγ flux

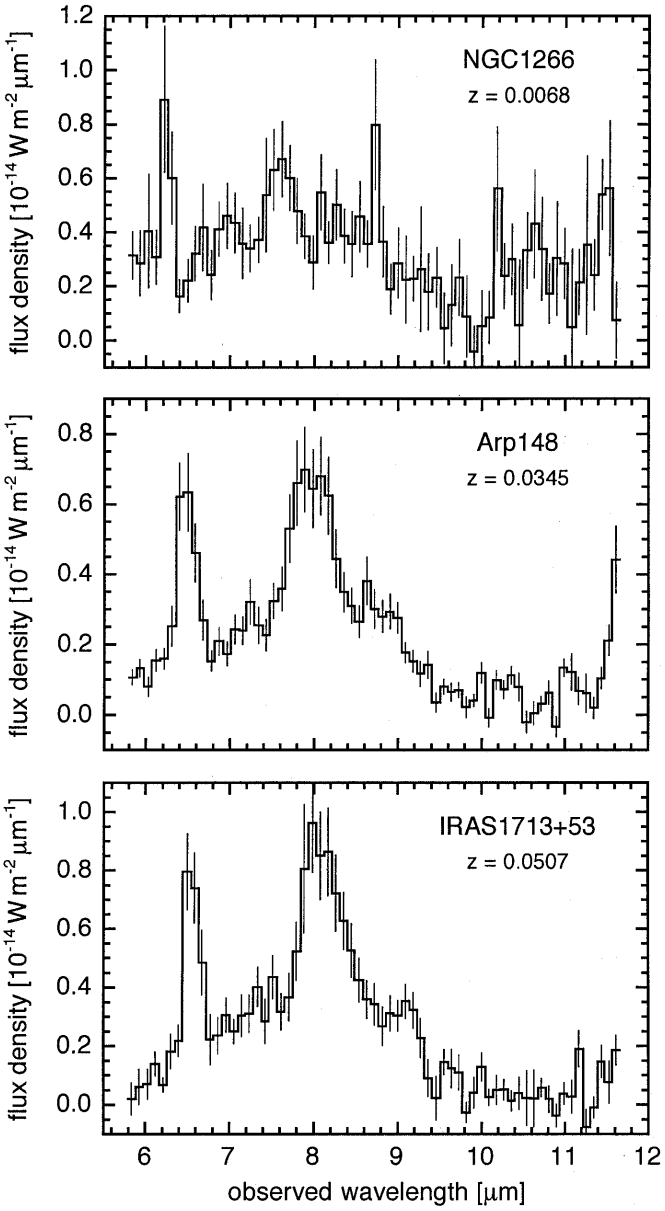

Fig. 2. The 6–12 μm spectra of NGC 1266 (top), Arp 148 (middle), and IRAS 1713+53 (bottom). We also present the redshift value (z).

($F_{\rm Br\gamma}$, Goldader et al. 1997a). The measurements of $F_{6.2}$ and $F_{\rm Br\gamma}$ are assumed to cover the whole starburst regions. Radio observations have revealed the predominance of compact ($\lesssim 5''$) sources in NGC 1266, Arp 148, and IRAS 1713+53 (Condon et al. 1990, 1991).

For reference, we use large-aperture data of M 82 (Willner et al. 1977; Satyapal et al. 1995). M 82 is an ideal standard of a starburst, where vigorous star formation dominates over the host galaxy (e.g., Moorwood 1996). Starbursts are expected to have nearly the same $F_{6.2}/F_{\rm IR}$ ratio if the extinction does not affect the 6.2 μm flux and an AGN does not contribute to the IR flux. This is because the flux ratio of the 3.28 μm feature to the IR continuum is constant among ordinary starburst galaxies (Mouri et al. 1990; Dennefeld & Désert 1990). In addition, Fig.

[2] The ISOPHOT Interactive Analysis is a joint development by the ESA Astrophysics Division and the ISOPHOT Consortium led by the Max Planck Institute for Astronomy (MPIA), Heidelberg. Contributing ISOPHOT Consortium institutes are DIAS, RAL, AIP, MPIK, and MPIA.

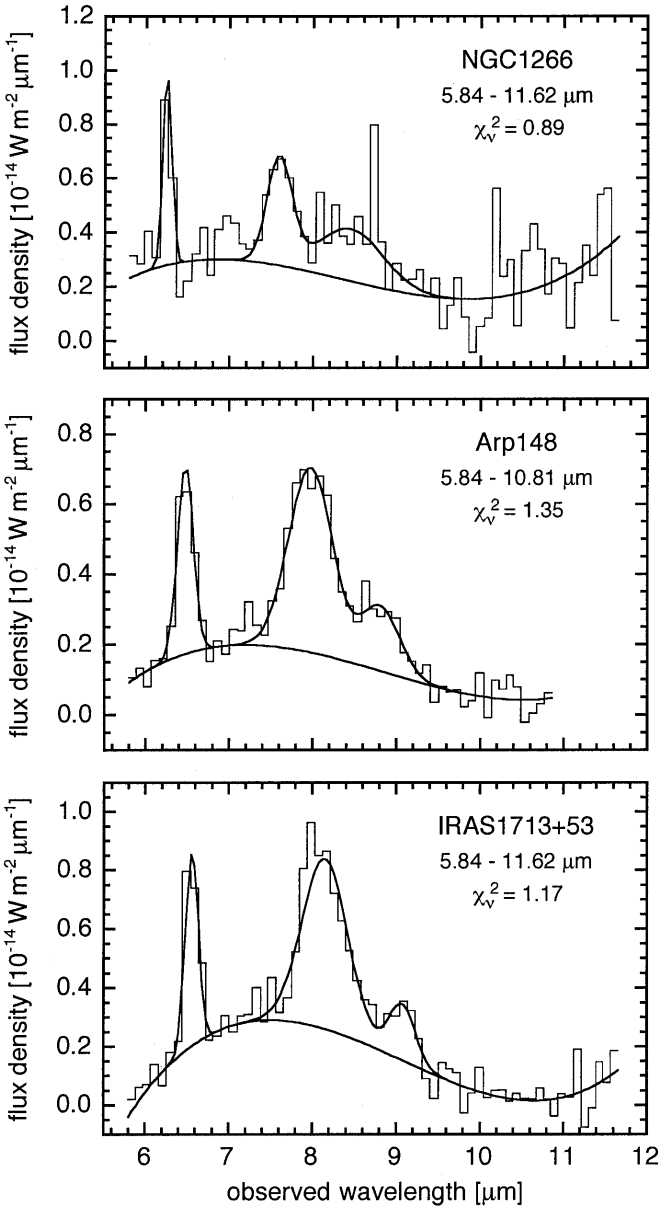

Fig. 3. The decomposition of the spectrum: NGC 1266 (top), Arp 148 (middle), and IRAS 1713+53 (bottom). Thick lines are the results for the continuum alone and the results for both the features and the continuum. Thin lines are the data. The wavelength range and the chi-square value normalized by the number of degrees of freedom (χ^2_ν) are also presented.

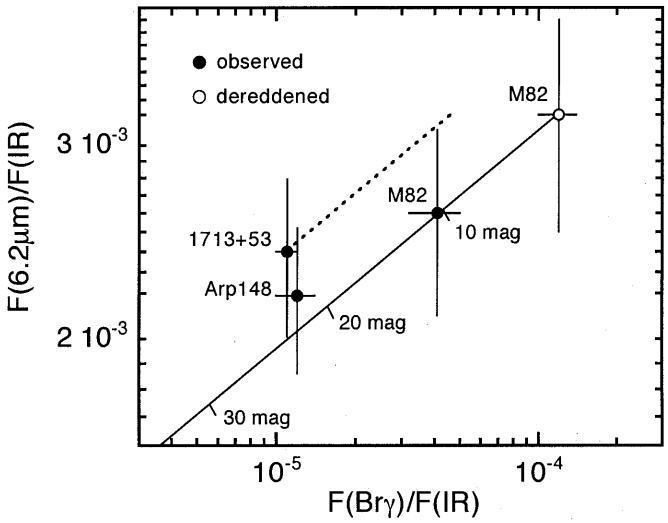

Fig. 4. Diagram of $F_{6.2}/F_{\rm IR}$ versus $F_{\rm Br\gamma}/F_{\rm IR}$. Filled circles stand for the observed data. An open circle stands for the dereddened data. A solid and a dotted lines illustrate the effect of extinction.

Table 1. Features in the spectra.

	NGC 1266	Arp 148	IRAS 1713+53
6.2 μm feature			
wavelength	6.21 ± 0.02	6.26 ± 0.01	6.24 ± 0.01
FWHM	0.12 ± 0.06	0.22 ± 0.03	0.18 ± 0.03
flux	0.94 ± 0.35	1.28 ± 0.19	1.29 ± 0.21
7.7 μm feature			
wavelength	7.54 ± 0.05	7.71 ± 0.03	7.76 ± 0.03
FWHM	0.35 ± 0.10	0.61 ± 0.07	0.64 ± 0.07
flux	1.46 ± 0.49	3.44 ± 0.39	3.94 ± 0.49
8.6 μm feature			
wavelength	8.39 ± 0.14	8.51 ± 0.05	8.64 ± 0.04
FWHM	0.91 ± 0.41	0.54 ± 0.12	0.37 ± 0.11
flux	1.87 ± 0.99	1.06 ± 0.25	0.74 ± 0.21

Notes.
1) The wavelength is with respect to the rest frame.
2) The wavelength and the full width at half maximum (FWHM) are in μm. The flux is in 10^{-15} W m^{-2}.

1b demonstrates a small dispersion in $12/FIR$ for the CfA starbursts; PAHs are the most plausible candidate for the 12 μm emitters (Puget & Léger 1989; Dennefeld & Désert 1990)[3].

Table 2 summarizes the data. The $F_{6.2}$ and $F_{\rm Br\gamma}$ values of M 82 have been corrected for extinction, by using the flux of the millimeter-wavelength recombination line H40α (Puxley et al. 1989). Fig. 4 compares $F_{6.2}/F_{\rm IR}$ with $F_{\rm Br\gamma}/F_{\rm IR}$. This diagram does not include NGC 1266, because the Brγ flux is not available. The solid line is the theoretical locus of M 82 for various amounts of extinction (Mathis 1990)[4]. Table 2 and Fig. 4 are used to discuss the starburst characteristics of the individual galaxies in the following subsections.

[3] There is also a contribution of hot dust particles within HII regions to the IRAS fluxes at 12 and 25 μm (Mouri et al. 1997). This component is ignored in the present discussion, because it is significant only in high-excitation starburst galaxies. See also Sect. 2.

[4] Lutz et al. (1996b) claim that the extinction at 4–8 μm is somewhat higher than assumed in Mathis (1990). This uncertainty in the extinction is not serious at our level of discussion, but might hamper the more detailed analyses.

Table 2. Summary of starburst properties.

	NGC 1266	Arp 148	IRAS 1713+53	M 82	
	observed	observed	observed	observed	dereddened
$L_{\rm IR}/L_{\odot}$	2.4 (10)	3.5 (11)	7.2 (11)	4.7 (10)	
$F_{6.2}/F_{\rm IR}$	9.0 ± 3.4 (-4)	2.19 ± 0.33 (-3)	2.40 ± 0.39 (-3)	2.6 ± 0.5 (-3)	3.2 ± 0.7 (-3)
$F_{{\rm Br}\gamma}/F_{\rm IR}$		1.2 ± 0.2 (-5)	1.1 ± 0.1 (-5)	4.1 ± 0.9 (-5)	1.2 ± 0.2 (-4)
$F_{6.2}/F_{12}$	2.2 ± 0.9 (-2)	4.3 ± 1.2 (-2)	4.3 ± 1.0 (-2)	1.9 ± 0.4 (-2)	

Notes.
1) The numbers in parentheses are decimal exponents.
2) The IRAS data are from Soifer et al. (1989). The Brγ fluxes of Arp 148 and IRAS 1713+53 are from Goldader et al. (1997a). The observed 6.2 μm flux of M 82 is adapted from Puget & Léger (1989) and Satyapal et al. (1995). The observed Brγ flux of M 82 is from Satyapal et al. (1995).
3) The dereddening of the M 82 data is based on the observed Brγ flux (Satyapal et al. 1995), the observed H40α flux (Puxley et al. 1989), the Case B approximation for $T_{\rm e} = 10^4$ K and $n_{\rm e} = 10^4$ cm^{-3} (Puxley et al. 1989), and the reddening law for $R_{\rm V} = 3.1$ (Mathis 1990).

Table 3. BGS galaxies with $C_{60} > 2.00$ and $\log(12/FIR) \leq -1.00$. The object names are the same as in Soifer et al. (1989) or Sanders et al. (1995).

name	$\log(L_{\rm IR}/L_{\odot})$	ref.	name	$\log(L_{\rm IR}/L_{\odot})$	ref.	name	$\log(L_{\rm IR}/L_{\odot})$	ref.
A0051–73	8.09	2	ESO320–G030	11.12	2	ESO453–G005	11.20	2
IR0136–10	11.74	1	IR1211+03	12.21	1	IR1713+53	11.86	1
IIIZw035	11.55	1	IR1222–06	11.11	1	IR17208–0014	12.38	2
IR0243+21	11.07	1	ESO507–G070	11.36	2	Zw083.025	10.90	2
NGC1266	10.38	1	IR13052–5711	11.17	2	IR17578–0400	11.31	2
IR0335+15	11.45	1	IR13120–5453	12.14	2	IR18587–1653	11.72	2
ESO203–IG001	11.77	2	IC860	11.02	1	IR19297–0406	12.35	2
IR05186–1017	11.21	2	ESO173–G015	11.42	2	IR19542+1110	12.05	2
NGC2623	11.50	1	UGC8696	12.11	1	UGC11898	10.99	2
IR09022–3615	12.21	2	IR1434–14	12.21	1	ESO239–IG002	11.76	2
IR09111–1007	11.97	2	IR14378–3651	12.09	2	IR2249–18	12.06	1
IR1017+08	11.72	1	Zw049.057	11.05	1	IR23365+3604	12.11	2
IR1056+24	11.95	1	IR1525+36	11.94	1			
A1101+41 (Arp148)	11.55	1	UGC9913	12.13	1			

References: (1) Soifer et al. (1989); (2) Sanders et al. (1995).

5.1. NGC 1266

This is a S0 galaxy with a close companion (e.g., Baan et al. 1992). The $F_{6.2}/F_{\rm IR}$ value of NGC 1266 is low by a factor of 3 with respect to the intrinsic value of M 82 (Table 2). Thus at least 30 % of the IR luminosity originates in OB stars. The actual starburst contribution could be much greater than this face value, because NGC 1266 is an OH absorber (Baan et al. 1992), where the nucleus is obscured by cold thick gas along the line of sight. If the entire IR luminosity is due to the burst of star formation, the extinction has to be as large as $A_{\rm V} \sim 60$ mag.

Fig. 2 shows that the continuum underlying the PAH features is relatively strong in NGC 1266. Since the IR luminosity of NGC 1266 is in the range of inactive galaxies (Table 2), the stellar light of the host galaxy could contribute to the observed continuum. Alternatively, there might exist some contribution from an obscured AGN.

5.2. Arp 148

This is a ring galaxy (e.g., Joy & Harvey 1987). The $F_{6.2}/F_{\rm IR}$ and $F_{{\rm Br}\gamma}/F_{\rm IR}$ values of Arp 148 are simultaneously reproduced by 20 mag of visual extinction from the intrinsic values of M 82, as demonstrated in Fig. 4. If this is the case, the entire IR luminosity of Arp 148 arises from star formation which is similar to that of M 82. We remark that Arp 148 is an OH megamaser (Baan et al. 1992). Since OH megamasers are pumped by IR radiation from dust particles (Skinner et al. 1997), it is natural to consider that the nucleus of Arp 148 is hidden in a thick cocoon of hot dust.

Baan (1989) noticed that OH megamasers exhibit IRAS spectra very close to blackbody. Thus OH megamasers like Arp 148, together with some OH absorbers like NGC 1266, make up an important subsample of obscured IR galaxies. The OH emission/absorption requires a large molecular column density toward the galaxy center; emission occurs in objects with

high effective IR temperatures while absorption in objects with low temperatures (see also Majewski et al. 1993).

5.3. IRAS 1713+53

This is a merging system (e.g., Goldader et al. 1997a). The Brγ flux is the sum over the two nuclei, both of which are covered by our measurement of the 6.2 μm flux. In Fig. 4, IRAS 1713+53 lies above the solid line. With respect to $F_{6.2}/F_{\rm IR}$, the $F_{\rm Br\gamma}/F_{\rm IR}$ ratio appears to be too small to be explained by the reddening of M 82. We suspect that ionizing stars, which are responsible for the Brγ emission, are deficient in IRAS 1713+53. Since ionizing stars are shorter-lived than non-ionizing stars, the face values of $F_{6.2}/F_{\rm IR}$ and $F_{\rm Br\gamma}/F_{\rm IR}$ are reproduced from an old starburst by 10–20 mag of visual extinction (a dotted line in Fig. 4). Goldader et al. (1997a) found that IRAS 1713+53 has exceptionally deep absorption features of CO at 2.3 μm. This characteristic is consistent with our idea, because CO features of IR galaxies arise from red supergiants formed in the burst 10^7 yr ago (Goldader et al. 1997b). Unfortunately, at the present stage, the photometric uncertainty of the ISOPHOT-SL is large, and we cannot draw any definitive conclusion.

5.4. Comment on the 12 μm emission

The 12 μm emission of starburst galaxies is usually ascribed to PAHs (Dennefeld & Désert 1990). If this is the case, all starbursts should exhibit the same $F_{6.2}/F_{12}$ ratio, where F_{12} is the monochromatic IRAS flux at 12 μm. The ratios $F_{6.2}/F_{12}$ observed in Arp 148 and IRAS 1713+53 are higher than that in M 82 (Table 2). The reason seems to be that, because of the silicate absorption at 9.7 μm, the extinction is more serious in the IRAS 12 μm band than it is at 6.2 μm (Mathis 1990). On the other hand, the $F_{6.2}/F_{12}$ ratio of NGC 1266 is comparable to that of M 82 (Table 2). The ratios $F_{6.2}/F_{12}$ and $F_{6.2}/F_{\rm IR}$ observed in NGC 1266 are unlikely to be explained simultaneously by the extinction towards the starburst region alone. We suppose an additional contribution of the host galaxy to the F_{12} value of NGC 1266 or a contribution of an obscured AGN to the F_{12} and $F_{\rm IR}$ values (Sect. 5.1).

6. Concluding remarks

Mid-infrared spectra at 6–12 μm have been presented for the moderate-luminosity IR galaxies NGC 1266, Arp 148, and IRAS 1713+53. Their IRAS spectra are indicative of heavy obscuration. We have detected prominent PAH features at 6.2, 7.7, and 8.6 μm, demonstrating the significance of starbursts.

Though the dust would be eventually swept from the nuclear regions by mass outflows and radiation of OB stars and supernovae, we are uncertain about the fates of those systems. They might evolve directly into ordinary starburst or Seyfert galaxies. Alternatively, they might evolve into warm IR galaxies like NGC 4418, which is considered as an initial, dust-enshrouded stage of a Seyfert (Kawara et al. 1990). We are also uncertain whether the evolution alters their luminosities or not. The same controversy exists about the evolution of ultraluminous IR sources (Majewski et al. 1993). The ISO has obtained spectra of many IR galaxies (e.g., Lutz et al. 1996a). We expect that these data would reveal the ultimate nature of obscured objects at all the IR luminosities.

Acknowledgements. We wish to thank the ISO team for realizing this wonderful project. The comments of the referee, D. Lutz, were helpful in revising the manuscript. We are also grateful to H. Kubotani, T. Kurokawa, H. Okuda, T. Tanabe, and T. Tsuji for assistance. This work was financially supported in part by Grant-in-Aids for the Scientific Research (No. 0704405) from the Japanese Ministry of Education, Science, Sports, and Culture. Y. Sato was supported by the Grant-in-Aids for JSPS Fellows by the Ministry.

Appendix

Table 3 presents all the BGS galaxies with $C_{60} > 2.00$ and $\log(12/FIR) \leq -1.00$. When the 12 μm flux is not detected, we adopt the criterion $\log(12/FIR) \leq -0.90$. We are not confident that those IRAS colors always reflect the obscuration of the energy source, and provide our list as a guide to further research on this issue.

References

Baan, W. A., 1989, ApJ 338, 804
Baan, W. A., Haschick, A., Henkel, C., 1992, AJ 103, 728
Balzano, V. A., 1983, ApJ 268, 602
Boulanger, F., Beichman, C., Désert, F.X., et al., 1988, ApJ 332, 328
Boulanger, F., Pérault, M., 1988, ApJ 330, 964
Boulanger, F., Reach, W. T., Abergel, A., et al., 1996, A&A 315, L325
Bregman, J. D., Allamandola, L. J., Tielens, A. G. G. M., Geballe, T. R., Witteborn, F. C., 1989, ApJ 344, 791
Cohen, M., Allamandola, L., Tielens, A. G. G. M., et al., 1986, ApJ 302, 737
Condon, J. J., Helou, G., Sanders, D. B., Soifer, B. T., 1990, ApJS 73, 359
Condon, J. J., Huang, Z.-P., Yin, Q. F., Thuan, T. X., 1991, ApJ 378, 65
Dennefeld, M., Désert, F. X., 1990, A&A 227, 379
Désert, F. X., Dennefeld, M., 1988, A&A 206, 227
Goldader, J. D., Joseph, R. D., Doyon, R., Sanders, D. B., 1997a, ApJS 108, 449
Goldader, J. D., Joseph, R. D., Doyon, R., Sanders, D. B., 1997b, ApJ 474, 104
Helou, G., Ryter, C., Soifer, B. T., 1991, ApJ 376, 505
Huchra, J., Burg, R., 1992, ApJ 393, 90
Huchra, J., Davis, M., Latham, D., Tonry, J., 1983, ApJS 52, 89
Joy, M., Harvey, P. M., 1987, ApJ 315, 480
Kawara, K., Taniguchi, Y., Nakai, N., Sofue, Y., 1990, ApJ 365, L1
Kessler, M. F., Steinz, J. A., Anderegg, M. E., et al., 1996, A&A 315, L27
Klaas, U., Acosta-Pulido, J. A., Ábrahám, P., et al., 1997, ISOPHOT-S: Capabilities and Calibration, available from ISO Science Operations Centre
Lemke, D., Klaas, U., Abolins, J., et al., 1996, A&A 315, L64
Lutz, D., Genzel, R., Sternberg, A., et al., 1996a, A&A 315, L137
Lutz, D., Feuchtgruber, H., Genzel, R., et al., 1996b, A&A 315, L269

Majewski, S. R., Hereld, M., Koo, D. C., Illingworth, G. D., Heckman, T. M., 1993, ApJ 402, 125
Mathis, J. S., 1990, ARA&A 28, 37
Moorwood, A. F. M., 1996, Space Sci. Rev. 77, 303
Mouri, H., Kawara, K., Taniguchi, Y., 1997, ApJ 484, 222
Mouri, H., Kawara, K., Taniguchi, Y., Nishida, M., 1990, ApJ 356, L39
Osterbrock, D. E., Martel, A., 1993, ApJ 414, 552
Press, W. H., Teukolsky, S. A., Vetterling, W. T., Flannery, B. P., 1992, Numerical Recipes, 2nd ed. Cambridge Univ. Press, New York
Puget, J. L., Léger, A., 1989, ARA&A 27, 161
Puxley, P. J., Brand, P. W. J. L., Moore, T. J. T., Mountain, C. M., Nakai, N., Yamashita, T., 1989, ApJ 345, 163
Rieke, G. H., 1988, ApJ 331, L5
Sanders, D. B., Egami, E., Lipari, S., Mirabel, I. F., Soifer, B. T., 1995, AJ 110, 1993
Sanders, D. B., Mirabel, I. F., 1996, ARA&A 34, 749
Sanders, D. B., Soifer, B. T., Elias, J. H., Neugebauer, G., Matthews, K., 1988, ApJ 328, L35
Satyapal, S., Watson, D. M., Pipher, J. L., et al., 1995, ApJ 448, 611
Skinner, C. J., Smith, H. A., Sturm, E., Barlow, M. J., Cohen, R. J., Stacey, G. J., 1997, Nat 386, 472
Soifer, B. T., Boehmer, L., Neugebauer, G., Sanders, D. B., 1989, AJ 98, 766
Thuan, T. X., Sauvage, M., 1992, A&AS 92, 749
Willner, S. P., Soifer, B. T., Russell, R. W., Joyce, R. R., Gillett, F. C., 1977, ApJ 217, L121